tvst

Special Issue

Intrinsic Morphologic and Physiologic Development of Human Derived Retinal Ganglion Cells In Vitro

Michael L. Risner[1], Silvia Pasini[1], Xitiz Chamling[2], Nolan R. McGrady[1], Jeffrey L. Goldberg[3], Donald J. Zack[2], and David J. Calkins[1]

[1] Vanderbilt Eye Institute, Department of Ophthalmology & Visual Sciences, Vanderbilt University Medical Center, Nashville, TN, USA
[2] Wilmer Eye Institute, Department of Ophthalmology, Johns Hopkins University School of Medicine, Baltimore, MD, USA
[3] Byers Eye Institute, Department of Ophthalmology, Stanford University School of Medicine, Palo Alto, CA, USA

Correspondence: David J. Calkins, Assistant Vice President for Research, Vanderbilt University Medical Center, The Denis M. O'Day Professor of Ophthalmology & Visual Sciences, Vice-Chairman and Director for Research, The Vanderbilt Eye Institute, Director, Vanderbilt Vision Research Center, AA7103 MCN/VUIIS 1161 21st Ave. S., Nashville, TN 37232, USA.
e-mail: david.j.calkins@vumc.org

Received: March 1, 2021
Accepted: April 21, 2021
Published: August 12, 2021

Keywords: retinal ganglion cells; stem cells; neuroregeneration; clustered regularly interspaced short palindromic repeats; glaucoma; development

Citation: Risner ML, Pasini S, Chamling X, McGrady NR, Goldberg JL, Zack DJ, Calkins DJ. Intrinsic morphologic and physiologic development of human derived retinal ganglion cells in vitro. Transl Vis Sci Technol. 2021;10(10):1, https://doi.org/10.1167/tvst.10.10.1

Purpose: Human retinal ganglion cells (hRGC) derived from human pluripotent stem cells are promising candidates to model, protect, and replace degenerating RGCs. Here, we examined intrinsic morphologic and physiologic development of hRGCs.

Methods: We used CRISPR-Cas9 to selectively express tdTomato under the RGC-specific promoter, BRN3B. Human pluripotent stem cells were chemically differentiated into hRGCs and cultured up to 7 weeks. We measured soma area, neurite complexity, synaptic protein, axon-related messenger RNA and protein, and voltage-dependent responses.

Results: Soma area, neurite complexity, and postsynaptic density protein 95 increased over time. Soma area and neurite complexity increased proportionally week to week, and this relationship was dynamic, strengthening between 2 and 3 weeks and diminishing by 4 weeks. Postsynaptic density 95 localization was dependent on culture duration. After 1 to 2 weeks, postsynaptic density 95 localized within somas but redistributed along neurites after 3 to 4 weeks. Axon initial segment scaffolding protein, Ankyrin G, expression also increased over time, and by 7 weeks, Ankyrin G often localized within putative axons. Voltage-gated inward currents progressively developed, but outward currents matured by 4 weeks. Current-induced spike generation increased over time but limited by depolarization block.

Conclusions: Human RGCs develop up to 7 weeks after culture. Thus, the state of hRGC maturation should be accounted for in designing models and treatments for optic neuropathies.

Translational Relevance: We characterized hRGC morphologic and physiologic development towards identifying key time points when hRGCs express mechanisms that may be harnessed to enhance the efficacy of neuroprotective and cell replacement therapies.

Introduction

Glaucoma has a complex origin, comprising many different forms. Across its various forms, the disease selectively targets retinal ganglion cells (RGC) and their axons that comprise the optic nerve. A critical risk factor for glaucoma is stress caused by sensitivity to intraocular pressure conveyed to RGC axons at the optic nerve head.[1,2] Glaucoma is a neurodegenerative disease clinically treated by decreasing the intraocular pressure. Despite hypotensive treatment efforts, as many as 50% of those with glaucoma will progressively lose vision.[3] For these patients, glaucoma continues to degrade the optic projection because additional treatments are not available. In these cases, neuroprotective and cell replacement therapies are appealing strategies to preserve or reestablish vision.[4–8]

Cell replacement therapy requires a composition analogous to innate cells to assume the function of dying cells or to serve as a vehicle to deliver neuroprotective factors to native RGCs undergoing degeneration.[9,10] Human pluripotent stem cells, including human embryonic stem cells (hESCs) and human induced pluripotent stem cells, are promising candidates for cell replacement and neuroprotective therapies. Human pluripotent stem cells can be engineered using CRISPR-Cas9 technology to selectively express a fluorescent reporter (e.g., tdTomato) under a RGC-specific endogenous promoter such as BRN3B, which is an early and enduring transcription factor relatively restricted to RGCs.[11–13] After selection, engineered human pluripotent stem cells can be chemically differentiated into human RGCs (hRGCs) and successfully transplanted into recipient retinas.[11,12,14]

Human RGCs may also be used to screen compounds for the treatment of optic neuropathies.[7] Because most optic neuropathies occur after maturation, it is important to understand the developmental progression of hRGC to define maturity. In culture, hRGCs intrinsically recapitulate development patterns of native RGCs, expressing similar genetic markers corresponding with maturation milestones.[11] These cells express proteins common to many innate RGCs, yet also display genetic heterogeneity, indicating multiple RGC types similar to the diversity noted in mammalian retinas.[11,15–19] During development in culture, hRGC neurites increase in number and length, and neurites can be guided to form axon-like processes.[11,20,21] Human RGCs produce excitatory responses to glutamatergic agonists, and GABA receptors intrinsically switch from excitatory to inhibitory, which is important for synaptic development.[11,14,16,22,23] Finally, hRGCs generate voltage-gated Na^+ (NaV) and K^+ (Kv)–dependent action potentials in response to direct current stimulation,[17,24] and these responses increase over culture duration.[11,25,26]

In this study, we investigated the intrinsic morphologic and physiologic development of hRGCs over an extended period. We examined hRGC soma and neurite maturation, axon initial segment (AIS) development, and voltage-gated channel responses from 1 up to 7 weeks. We found soma size and neurite complexity linearly increased from 1 to 4 weeks in culture. Although soma size and neurite complexity increased proportionally week to week, this relationship is dynamic, increasing in strength between 2 and 3 weeks in culture and decreasing after 4 weeks. Like the dynamic relationship between soma size and neurite complexity, expression patterns of postsynaptic density protein 95 (PSD-95) changes over culture duration. After 1 week in culture, we found PSD-95 concentrated in somatic cytoplasm with sparse localization within neurites. After 4 weeks, somatic PSD-95 localization decreased, whereas PSD-95 increased along neurites. We also probed for the AIS scaffolding protein, Ankyrin G (AnkG), which is a key regulator of neuron polarity.[27,28] After 1 week in culture, AnkG expression is minimal. After extending the culture period to 7 weeks, we observed that AnkG accumulated in somas and along putative axons. As the axon-like neurite developed, so too did NaV and Kv channel responses and spike activity.

Methods

Human RGC Recovery and Culture

BRN3B-H9 reporter hESCs were generated by Dr Donald Zack's laboratory at Johns Hopkins University.[11,12] BRN3B-H9 cells were shipped frozen to Vanderbilt University Medical Center, and we quickly thawed and plated hRGCs on glass coverslips at the density of 60,000 cells/cm^2. Before plating, coverslips were coated with 0.1 mg/mL poly-D-lysine (Sigma, St. Louis, MO) dissolved in 100 mM sodium borate buffer (VWR International, Radnor, PA) for 2 hours at room temperature followed by 5 µg/mL mouse laminin (Sigma) dissolved in DMEM/F12 (Thermo Fischer Scientific, Waltham, MA) media overnight at 37°C. The hRGCs were plated and maintained in iNS media composed of 1:1 mix of Neurobasal and DMEM/F12 media, 1× GlutaMAX Supplement, 1× antibiotic–antimycotic,1% N2 Supplement, and 2% B27 Supplement (Thermo Fischer Scientific). We completely replaced the media 24 hours after plating and refreshed one-half of the media twice a week until each experimental end point.

Human RGC Messenger RNA Expression Measurement

The messenger RNA expression values were obtained from the RNA sequencing performed on the hESC-RGC.[12] Briefly, the BRN3B-H9 reporter hESCs were differentiated to RGCs for 40 days on neural induction media.[12] On day 40 of differentiation, two independent batches of BRN3B-tdTomato+ RGCs were purified using magnetic activated cell sorting.[12] RNA was extracted from the purified RGC population using RNAeasy plus kit (Qiagen, Hilden, Germany). Complementary DNA synthesis was performed using SuperScript III Synthesis SuperMix (Thermo Fischer Scientific), and a complementary library was prepared

using the Nextera DNA Library Preparation Kit (Illumina, San Diego, CA). Libraries were then multiplexed and sequenced on an Illumina MiSeq with 76 bp paired end reads to an average depth of approximately 8 million paired end reads per sample. Reads were aligned to Gencode Release 24 (GRCh38.p5) using HISAT2 (v2.0.1-beta).[29] Cuffquant and Cuffnorm (Cufflinks v2.2.1) were used to quantify expression levels and to calculate normalized fragments per kilobase million values.[30]

Human RGC Electrophysiology

After culture, we transferred hRGCs and culture media into a physiologic chamber attached to an upright microscope stage (Olympus BX50). We adhered hRGC coverslips to the physiologic chamber using vacuum grease. We gradually replaced culture media with bicarbonate-buffered Ames' media supplemented with 20 mM glucose and progressively heated to approximately 32°C (Model TC-344C, Warner Instruments, Hamden, CT). For whole cell recordings, we used borosilicate glass patch pipettes filled with (in mM): 100 $KMeSO_4$, 5 KCl, 5 NaCl, 10 HEPES, 4 EGTA, 10 Na-Phosphocreatine, 4 Mg-ATP, 0.4 Na-ATP, and 0.1 Lucifer yellow. Intracellular solution osmolarity was 280 Osm with a pH of 7.3. Patch pipette resistance ranged from 3.5 to 6.5 MΩ. Electrical signals were recorded (Multiclamp 700B, Molecular Devices, San Jose, CA) and digitized at a sampling rate of 10 kHz or greater (Digidata 1550A, Molecular Devices). Patch pipette potential was held at –60 mV during formation of a 1 GΩ or higher seal, and the cell membrane was perforated by manually applying brief negative pressure pulses. The whole cell configuration was determined by a change in access resistance and verified by transmission of Lucifer Yellow into the cell by exciting the dye with 405 nm (pE-4000, CoolLED, Andover, UK). After attaining whole-cell configuration, we measured resting membrane potential in current-clamp mode (0 pA) within the first 2 minutes. Human RGC resting membrane potential remained depolarized compared with typical RGCs from acutely dissected whole retinas.[31–33] Thus, we often hyperpolarized cells to –60 mV by current injection to measure spontaneous and current-driven spiking. We measured current-evoked spiking by injecting 1 s hyperpolarizing and depolarizing currents from a holding potential of –60 mV. We assessed activation of voltage-gated Na^+ (NaV) and K^+ (Kv) channels by depolarizing the membrane potential from –80 to +30 mV in 10-mV increments (50 ms duration) from a holding potential of –80 mV. We determine NaV channel availability by inactivating channels with conditioning potentials from –100 to –20 mV (in 10-mV increments, 500 ms duration) from a holding potential of –80 mV, and we determined channel availability by injecting a brief (40 ms) –10 mV test potential. Ionic currents were isolated by subtracting capacitive and leak currents evoked by six hyperpolarizing potentials after each test potential. We analyzed electrophysiologic data using Clampfit 11.1 (Molecular Devices).

Human RGC Immunocytochemistry and Neuritic Morphology Analysis

After electrophysiologic recordings, hRGCs were fixed with 4% paraformaldehyde overnight at 4°C and immunolabeled with the following primary antibodies: RNA-binding protein with multiple splicing (RBPMS, GTX118619,1:200, Genetex, Irvine, CA) postsynaptic density 95 (PSD-95, APZ-009, 1:400, Alomone Labs, Jerusalem, Israel), and AnkG (338800, 1:250, Invitrogen, Carlsbad, CA). Human RGCs were then incubated with appropriate secondary antibodies for 2 hours at room temperature (1:200; Jackson ImmunoResearch Laboratories, Inc., West Grove, PA) and cover slipped with Fluoromount G (Southern Biotech, Birmingham, AL). We imaged hRGCs with an Olympus FV-1000 inverted confocal microscope. Images were analyzed using Fiji ImageJ Version 1.53c. We manually counted the number of primary and secondary neurites. We measured PSD-95 and AnkG immunolabeling in somas and neurites using freehand selection and segmented line tools in ImageJ.

Statistical Analysis

We quantified data using Graphpad Version 8.3 (Graphpad Software LLC., San Diego, CA). We first determined if datasets formed a normal distribution using Shapiro-Wilk tests. If datasets were normally distributed, we performed parametric statistics; otherwise, we performed non-parametric statistics. We defined statistical significance as a P value of 0.05 or less.

Results

Dynamic Relationship Between Soma and Neurites During Development

We confirmed putative tdTomato-positive hRGCs by immunolabeling against RBPMS (Fig. 1A).[34] RBPMS labeling intensity proved variable, but we found 96.5 ± 1.5% of tdTomato-positive cells co-expressed RBPMS. Similar to an earlier report,[26]

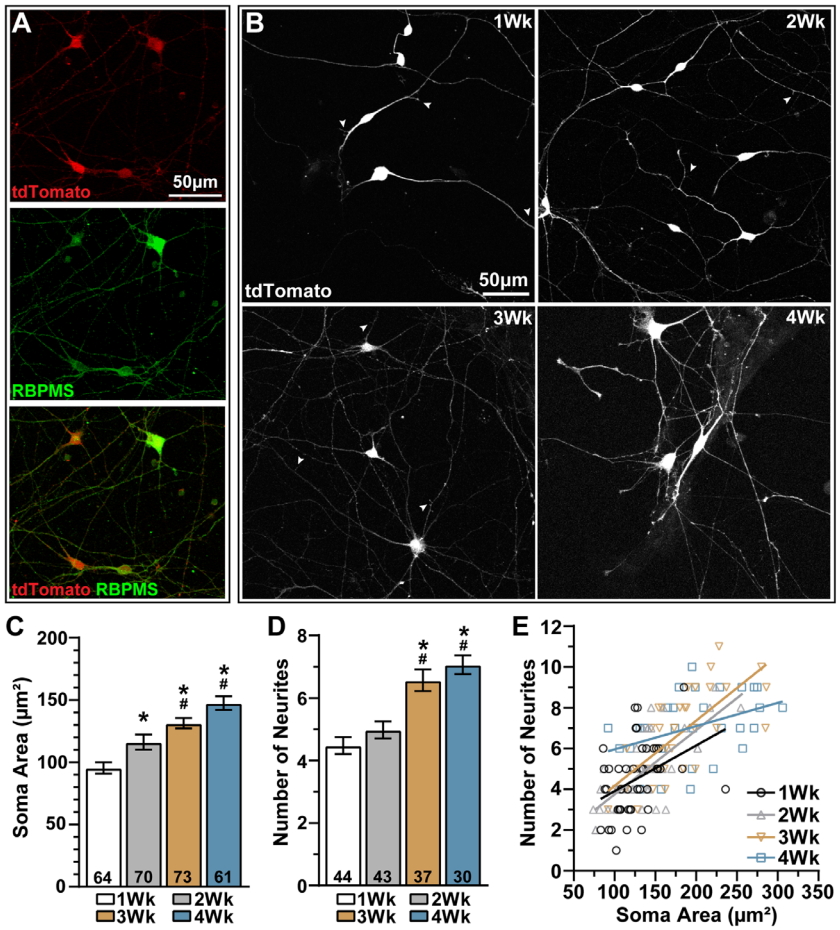

Figure 1. hRGC confirmation and somatoneuritic development. (**A**) Example BRN3B-positive hRGCs expressing tdTomato (red) immunolabeled against RBPMS (green) after 4 weeks in culture. Scale bar = 50 µm. We found 96.5% of tdTomato-positive cells co-expressed RBPMS. We included 167 cells from 10 samples. (**B**) Representative tdTomato-positive (grayscale) hRGCs after 1 to 4 weeks in culture. Arrowheads indicate putative filopodia. Scale bars = 50 µm. (**C**) Soma size ($P \leq 0.012$) and (**D**) number of neurites ($P \leq 0.007$) significantly increase over culture duration. (**E**) The positive relationship ($P \leq 0.03$) between soma size and neurite number dynamically changes over culture duration (1Wk $R^2 = 0.14$, 2Wk $R^2 = 0.52$, 3Wk $R^2 = 0.54$, 4Wk $R^2 = 0.16$). Statistic: Kruskal-Wallis, Dunn's post hoc test (**C**, **D**). *Significantly different versus 1-week cells, #significantly different compared with 2-week cells, Linear regression (**E**), test of slopes (**E**). Data are mean ± standard error of the mean.

we noticed hRGC somas and neurites increased in size and complexity over culture duration (Fig. 1B). This intrinsic and ongoing development is demonstrated by filopodia extending from neurites, signifying active synaptogenesis (Fig. 1B, arrowheads).[21,35] When quantified, we found cross-sectional soma area increased from week to week ($P \leq 0.012$), increasing by 54% between 1 (95 ± 4.5 µm^2) and 4 (147 ± 5.4 µm^2) weeks in culture ($P < 0.001$) (Fig. 1C). Like the soma area, the number of primary and secondary neurites also increased with time in culture from 4.5 ± 0.27 at 1 week to 7.1 ± 0.3 neurites at 4 weeks ($P < 0.001$) (Fig. 1D).

We then quantified the relationship between soma area and neurite complexity during culture (Fig. 1E). After 1 week, we found a positive ($P = 0.01$), albeit weak ($R^2 = 0.14$), correlation between soma area and neurite number. After 2 to 3 weeks, the positive ($P < 0.001$) relationship between the soma area and the neurite number increased in strength ($R^2 \geq 0.52$), and the rate of change between the soma area and the neurite number significantly increased compared with cells at 1 week ($P \leq 0.012$). By 4 weeks, the positive correlation ($P = 0.03$) between soma area and neurite complexity decreased ($R^2 = 0.16$), and the rate of change between soma area and neurite number decreased below that of cells at 1 week, indicating neurite refinement ($P = 0.002$).

Based on our finding that neurite complexity increases over time (Figs. 1D, E), we anticipated

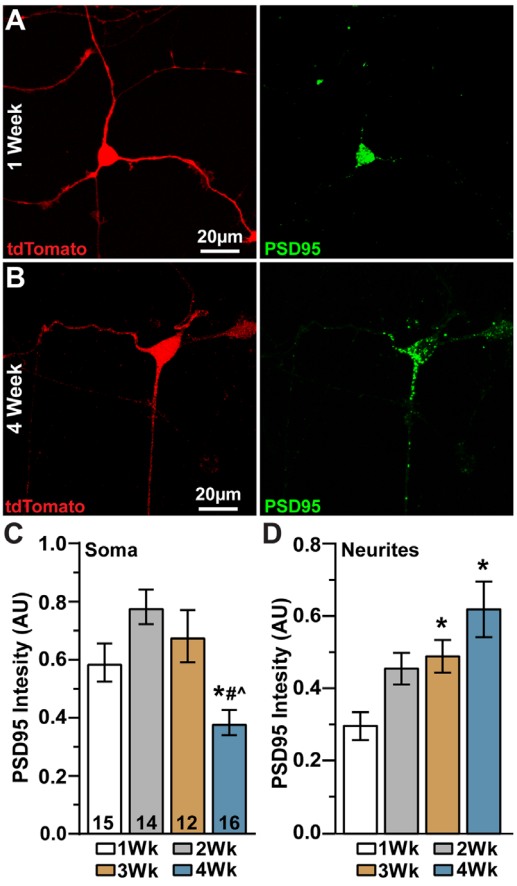

Figure 2. PSD-95 expression pattern depends on culture duration. (**A**, **B**) Representative tdTomato-positive hRGCs (*red*) cultured for 1 (**A**) and 4 (**B**) weeks and immunolabeled against PSD-95 (*green*). Scale bar = 20 µm. (**C**) PSD-95 labeling within hRGC somas significantly decreased after 4 weeks versus earlier time points ($P \leq 0.033$). (**D**) Quantification of PSD-95 labeling within hRGC primary neurites. PSD-95 labeling significantly increased by 3 and 4 weeks in culture compared with 1-week cells. Significance indicators: * comparison with 1-week cells, # comparison with 2-week cells, ^ comparison with 3-week cells. Statistics: one-way analysis of variance, Tukey post hoc test (**C**, **D**). Data are mean ± standard error of the mean.

synaptic proteins too would increase. To test this notion, we labeled cells against PSD-95 and analyzed the intensity within the hRGC somas and primary neurites after 1 to 4 weeks. After 1 week in culture, PSD-95 seemed to be concentrated within the hRGC somas with sparse labeling throughout the neurites (Fig. 2A). At 4 weeks after culture, somatic PSD-95 labeling seemed to be punctate yet increased within neurites (Fig. 2B). When quantified, we found PSD-95 labeling within somas significantly decreased after 4 weeks in culture compared with earlier time points ($P \leq 0.033$) (Fig. 2C). In contrast, we found PSD-95 labeling along neurites significantly increased in 3- and 4-week hRGCs compared with 1-week cells ($P \leq 0.035$) (Fig. 2D).

Voltage-Gated Responses Mature Along with AIS Localization

The somatodendritic compartment is separated from the axon by the axon initial segment (AIS). As its spatial position suggest, the AIS is essential for the maintenance of neuron polarity.[28,36] The AIS is identified by the scaffolding protein, AnkG, and the encoding gene for AnkG, ANK3, is abundantly expressed in hRGCs along with other AIS-related genes (Fig 3A). Moreover, genes encoding voltage-gated ion channels essential for AIS formation are also expressed in hRGCs (Fig. 3B).[36] To determine the expression pattern of AnkG over culture duration, we immunolabeled cells against AnkG and measured the intensity of AnkG labeling within the soma and putative axon. We identified the putative axon based on AnkG-positive immunolabeling. For cases where AnkG labeling was not observed, we defined the putative axon as the longest neurite. After 1 week in culture, we typically found only modest AnkG protein expression in hRGCs independent of compartment (Figs. 3C, E, F). However, after 7 weeks in culture, AnkG accumulated in the cytosol and along the putative axon (Figs. 3D, E, F). When quantified, we found AnkG immunolabeling within the soma increased by 65% from 1 to 7 weeks in culture ($P = 0.003$) (Fig. 3G). AnkG also significantly accumulated within putative axons over the culture duration, increasing by 53% ($P = 0.039$) (Fig. 3H). Although AnkG increases in somas and putative axons over time, the ratio of AnkG labeling in axons and somas does not change, indicating a progressive and equal accumulation of the protein within each compartment ($P = 0.68$) (Fig. 3I).

Human RGCs intrinsically express genes encoding voltage-gated Na^+, K^+, and Ca^{2+} channels (Fig. 3B). Because these channels localize within the AIS or dendrites of native RGCs,[37–40] we expected voltage-gated response would also mature with time in culture. We tested this notion by targeting tdTomato-positive hRGCs for whole cell recording after 1 to 7 weeks in culture. We confirmed the whole cell configuration based on a change in access resistance and transmission of Lucifer yellow into the cell (Fig. 4A). We observed variability in dendritic complexity, spontaneous spiking, and voltage-gated responses among hRGCs within the same culture slide and between time points (Figs. 4B, C). Despite this variability, we noticed hRGCs that had more complex dendritic organization often produced spontaneous firing and larger inward currents (Figs. 4B, C).

Next, we characterized hRGC responses to a series of hyperpolarizing and depolarizing current injections (–20 to +100 pA in +10-pA increments) after 1 to

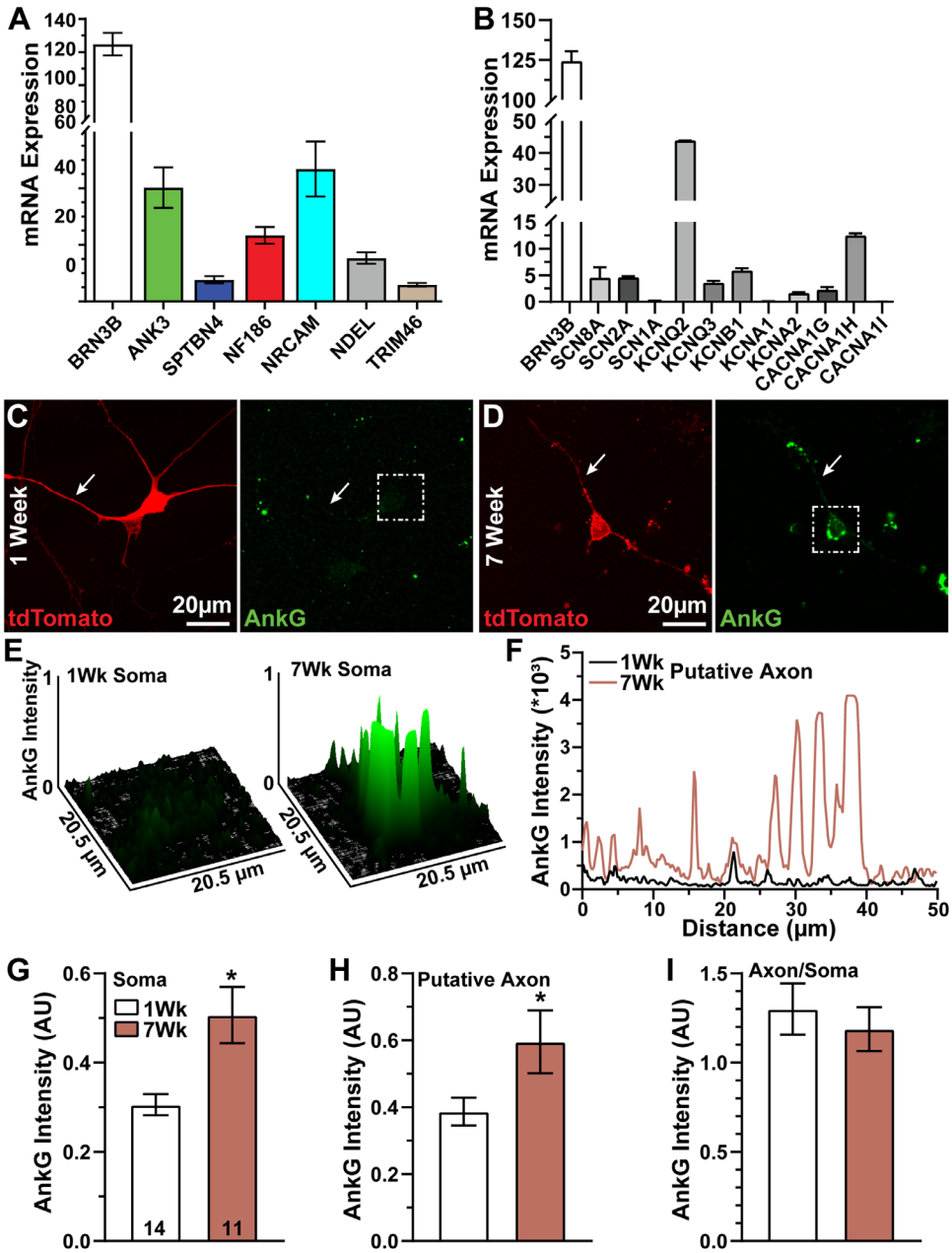

Figure 3. AnkG expression increases over time. (**A**) Messenger RNA (mRNA) expression (fragments per kilobase million) of BRN3B- and AIS-related genes in hRGCs. (**B**) mRNA expression of BRN3B and select voltage-gated ion channel genes. (C, D) Representative tdTomato-positive (*red*) hRGCs after 1 and 7 weeks in culture immunolabeled against AnkG (*green*). *Arrows* indicate axon-like neurites. Putative axon was identified by AnkG localization or as the longest neurite. Scale bars = 20 µm. (**E**) Surface plot of AnkG intensity distribution in somas indicated by *dashed boxes* above (**C**, **D**). (**F**) AnkG fluorescence intensity profiles along axon-like neurites indicated above (**C**, **D**). Quantification of AnkG immunolabeling within hRGC (**G**) somas and (**H**) putative axons relative to tdTomato intensity. AnkG localization significantly increases within somas ($P = 0.003$) and putative axons ($P = 0.039$) after 7 weeks in culture. (**I**) However, the ratio of AnkG labeling in putative axons and somas (axonal divided by somatic AnkG intensity) does not change between 1 and 7 weeks ($P = 0.68$). Statistics: *t*-test (**G**, **H**), Mann-Whitney *U* test (**I**). Data presented as mean ± standard error of the mean.

7 weeks in culture. We clamped hRGCs at –60 mV because the resting membrane potential was typically too depolarized (–40.0 ± 0.9 mV) for cells to generate full action potentials.[25] After 1 week in culture, hRGCs typically produced single spikes that often failed to completely repolarize in response to modest depolarizing current injections (Fig. 5A, left). By 4 weeks, hRGCs generated multiple spikes in response

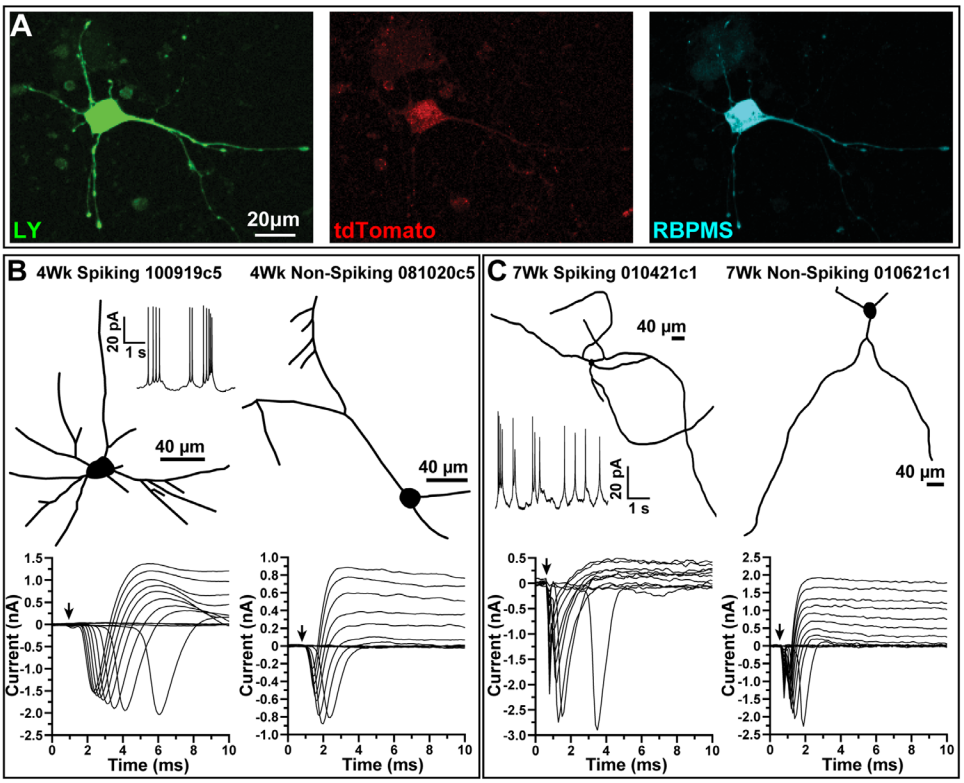

Figure 4. Structure-Function Comparison of hRGCs. (**A**) We targeted tdTomato-positive (*red*) hRGCs for whole-cell recordings and dye loading with Lucifer yellow (LY). For some experiments, we confirmed hRGCs by immunolabeling against RBPMS (*cyan*). Following physiology, we recovered morphology of LY-labeled hRGCs using fluorescence microscopy, and we manually traced the somato-neurite compartments. (**B**, **C**) Comparison of somato-neurite morphology and voltage-gated responses of spontaneously spiking versus non-spiking cells after 4 (**B**) and 7 (**C**) weeks in culture. *Arrows* indicate stimulus onset.

to small current injections (approximately 10 pA), but larger currents (20–100 pA) often elicited fewer spikes followed by aborted action potentials (Fig. 5A, middle). After 7 weeks, hRGCs produced a volley of repetitive spikes that quickly polarized and repolarized in response to small currents, but again, larger currents evoked few full spikes at stimulus onset followed by aborted spikes or maintained membrane depolarization during stimulation (Fig. 5A, right). In contrast with the weak responses of hRGCs to depolarizing currents after 1 week in culture, responses to the relief of hyperpolarizing currents (rebound excitability) are more robust (Fig. 5B, left). This finding is consistent with expression of CACNA1H (CaV3.2) (Fig. 3B).[40–42] By 7 weeks in culture, hRGC rebound excitability seemed to strengthen (Fig. 5B, right).

Overall, we found the percent of cells producing spontaneous or evoked action potentials increased over culture duration from 29% at 1 week, 67% at 4 weeks, and 70% at 7 weeks (Fig. 5C). For hRGCs producing one or more spike(s), we quantified the spike rate generated for each test current. We found 7-week cells produced significantly greater rebound excitability compared with 4-week cells ($P < 0.05$) (Fig. 5D). In response to depolarizing current injections, hRGCs cultured for 4 and 7 weeks produced greater responses than 1-week cells to larger test pulses ($P \leq 0.03$) (Fig. 5D). Finally, we determined the hRGC spike threshold, which was defined at the inflection point before the upstroke in response to the minimum depolarizing current evoking at least one spike (i.e., rheobase).[43] We found that spike threshold significantly decreased from –37 ± 1 mV at 1 week to –42.5 ± 1.2 mV at 4 weeks ($P = 0.028$) and decreased further after 7 weeks in culture to –48.3 ± 1 mV ($P \leq 0.002$) (Fig. 5E).

Based on our findings that the spike rate increased and the spike threshold decreased with culture duration (Figs. 5D, E), we expected NaV and Kv conductance so too would increase over time. We tested this idea by voltage-clamping cells at –80 mV and depolarizing cell membranes with brief, 50 ms, test potentials from –80 to +30 mV (Fig. 6A, inset). We noticed that NaV-mediated fast inward currents and Kv outward currents increased over culture duration (Figs. 6A–D).

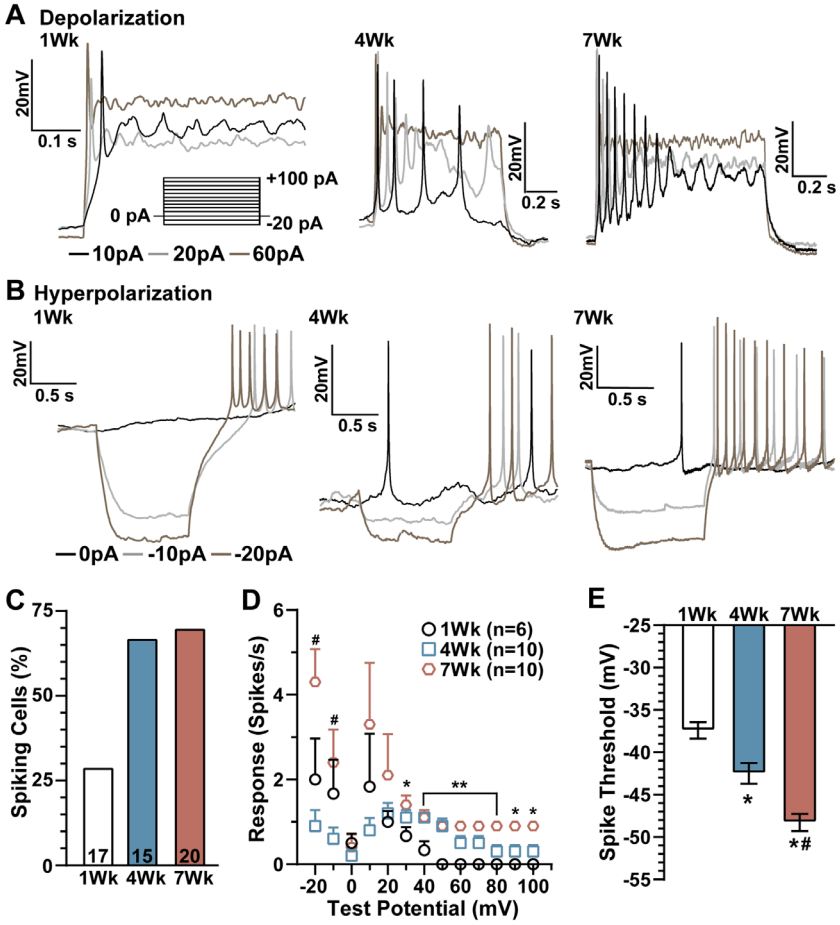

Figure 5. hRGC excitability increases as spike threshold decreases. (**A**, **B**) Example responses from hRGCs after 1, 4, and 7 weeks in culture to a series of depolarizing (**A**) and hyperpolarizing (**B**) current injections from a holding potential of –60 mV. (**C**) Percent of hRGCs generating spontaneous or stimulus-induced spiking. (**D**) Quantification of spike rate for 1-, 4-, and 7-week hRGCs in response to a series of depolarizing and hyperpolarizing current injections (**A**, **B**). Compared with 1-week cells, hRGCs cultured for 4 and 7 weeks were more likely to produce action potentials in response to larger depolarization currents (30–100 pA, *7Wk vs. 1Wk $P \leq 0.032$, **4Wk and 7Wk vs.1Wk; $P \leq 0.05$). hRGCs cultured for 7 weeks produced more robust responses after hyperpolarizing currents compared with 4-week cells (#, $P \leq 0.05$). (**E**) Spike threshold significantly decreased over culture duration: * 1Wk vs. 4Wk $P = 0.028$, * 1Wk vs. 7Wk $p<0.001$, # 4Wk vs. 7Wk $P = 0.0023$. Statistics: mixed effects repeated measures analysis, Benjamini, Krieger, and Yekutieli post hoc tests (**D**), one-way analysis of variance, Tukey post hoc test (**E**). Data are mean ± standard error of the mean.

After 1 to 3 weeks, hRGC inward currents increased in response to –40 mV (Fig. 6E), similar to their spike threshold potential (Fig. 5E). Again, similar to our finding that spike threshold decreased over time in culture, inward currents from 4- and 7-week cells activated at smaller test potentials (approximately –50 mV) (Fig. 6E). We also found that the inward currents peaked at lower test potentials in hRGCs cultured for 4 and 7 weeks (–40 mV) compared with 1- to 3- week cells (–20 to –30 mV) (Fig. 6E). Overall, the inward current continually grew larger with each subsequent week in culture after 2 weeks ($P \leq 0.038$). As Kv channel activation accumulated at more positive test potentials (–30 to –40 mV), inward currents produced by hRGCs cultured for 1 to 4 weeks grew smaller (Fig. 6E). However, the 7-week hRGC responses deviated from this standard, slightly increasing in amplitude from +10 to +30 mV (Fig. 6E).

Inward current conductance seems to continually develop, whereas the mechanisms driving the outward current mature by 4 weeks in culture (Fig. 6F). For cells cultured 4 to 7 weeks, we did not observe a difference in the outward current peak response regardless of test potential ($P \geq 0.27$). Even by 3 weeks in culture, hRGCs typically produced significantly larger outward currents in response to larger (–20 to +30 mV) test potentials compared with 1- or 2-week cells ($P \leq 0.02$). After 4 to 7 weeks in culture, hRGC outward current

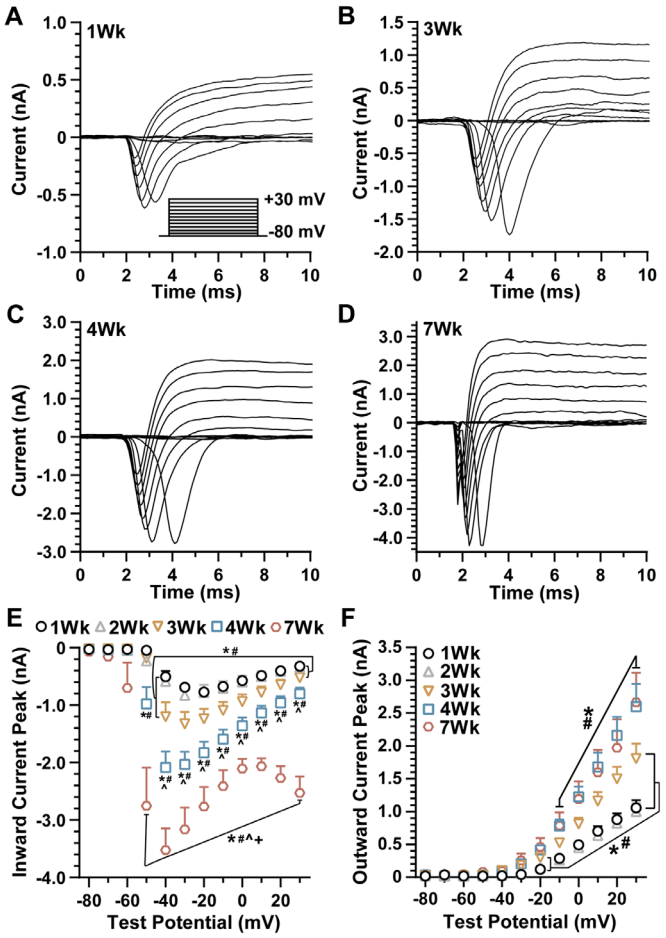

Figure 6. Voltage-gated responses increase over time. (**A**–**D**) Example voltage-gated responses of hRGCs cultured for 1, 3, 4, and 7 weeks to depolarizing potentials (50 ms duration) of –80 to +30 mV in 10-mV increments from a holding potential of –80 mV. (**E**) Inward and (**F**) outward currents of hRGCs significantly increase over culture duration. (**E**) Inward current significance indicators: * vs. 1Wk $P \leq 0.038$; #, s. 2Wk $P \leq 0.025$; ^ vs. 3Wk $P \leq 0.016$; and + vs. 4Wk $P \leq 0.015$. (**F**) Outward current significance indicators: * vs. 1Wk $P \leq 0.041$ and # vs. 2Wk $P \leq 0.042$. Number of cells per group: 1Wk: $n = 13$, 2Wk: $n = 31$, 3Wk: $n = 19$, 4Wk: $n = 16$, 7Wk: $n = 6$. Statistics: Two-way repeated measures analysis of variance, Benjamini, Krieger, and Yekutieli post hoc tests (**E**, **F**). Data presented as mean ± standard error of the mean.

peaks grew significantly larger than 1- or 2-week cells beginning at –10 mV and extending to +30 mV ($P \leq 0.042$) (Fig. 6F).

As noted elsewhere in this article, hRGCs tend to produce few repetitive spikes in response to modest levels of direct current stimulation and membrane potential remains depolarized (Fig. 5A). This type of response, termed depolarization block, has been suggested to be cause by inactivation of NaV channels.[21] To test this idea, we voltage-clamped cells at –80 mV, gradually inactivated NaV channels with conditioning voltage steps from –100 to –20 mV for 500 ms, and then injected a brief (40 ms) depolarizing test potential (–10 mV) to determine the remaining fraction of NaV channels available (Fig. 7A).[44] As expected, hRGCs cultured longer produced larger inward currents in response to the test potential following conditioning potentials, ranging from –100 to –50 mV ($P \leq 0.043$) (Fig. 7B). However, after normalization, we found the number of channels available decreased at a lower conditioning potential (–50 mV) for 7-week cells compared with cells cultured for 1 to 4 weeks ($P \leq 0.047$) (Fig. 7C).

Discussion

Human RGC Soma and Neurite Development

We find that 96.5% of tdTomato-positive hRGCs co-express the RGC-specific marker, RBPMS (Fig. 1A). Our result confirms and extends the notion that hRGCs are akin to innate RGCs.[7,12,17,45] Human RGC somatic and neuritic compartments rapidly develop in culture.[26] A recent report noted that, at 1 day after differentiation, hRGC soma area is about 45 μm^2, and 75 μm^2 after 7 days.[26] Our results indicate that hRGCs are slightly larger after 1 week in culture (95 μm^2), but similar to other reports,[26] hRGC somas grow increasingly larger over culture duration (Fig. 1B, C). Human RGC primary and secondary neurites also increased in number during culture from an average of 4.5 at 1 week to 7.0 at 4 weeks (Fig. 1D). Others have found hRGCs are intrinsically more complex after 7 days in culture (about seven primary and secondary neurites), but similar to our results, neuritic complexity also increases with time.[26]

Soma size and dendritic complexity of native RGCs are positively correlated,[46] a finding we confirm for hRGCs (Fig. 1E). We also find the strength of the relationship between soma area and neurite density changes during development. After 2 to 3 weeks, we found soma area and neurite number are moderately correlated (Fig. 1E). After 4 weeks, the strength of this relationship is significantly diminished (Fig. 1E). Based on this broad measurement, hRGCs seem to undergo active dendritic refinement like that observe in the developing retina.[21,35,47]

Human RGCs demonstrate neurite refinement (Fig. 1E) and increased synaptic protein expression as observed in postnatal brain development.[26,48] PSD-95 is a synaptic scaffolding protein that recruits and anchors glutamate and ion channels, which is essential during synaptic plasticity.[49,50] Because hRGCs produce excitatory inward currents in response to glutamate and kainite,[11,16] we anticipated PSD-95

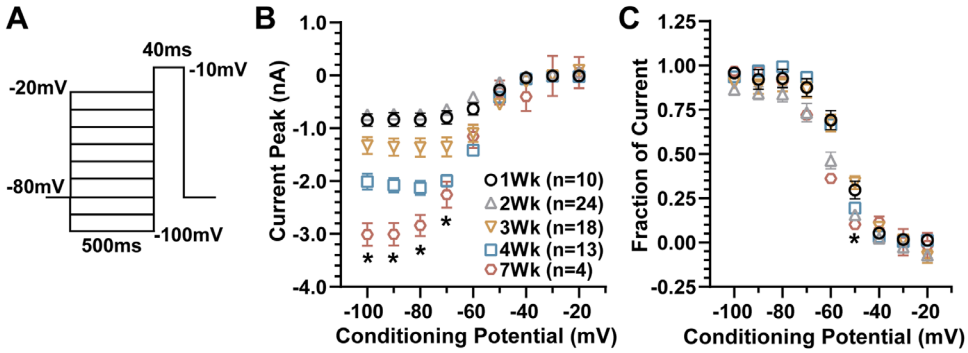

Figure 7. Development of inactivation in hRGCs. (**A**) hRGCs were voltage clamped at –80 mV, held at conditioning voltage steps (from –100 to –20 mV, in 10-mV increments) for 500 ms, and then depolarized by a brief (40 ms) test potential (–10 mV) to determine the fraction of available channels after each conditioning potential. (**B**) Averaged responses produced by the test potential after each conditioning potential. hRGCs cultured 7 weeks consistently produced significantly larger responses to the test potential after –100 to –70 mV conditioning potentials compared with hRGCs cultured for 1 and 2 weeks (*$P \leq 0.05$). (**C**) For each cell, responses to the test potential were normalized by dividing by the maximum response. After 7 weeks in culture, inactivation significantly accumulated after the –50 mV conditioning potential compared with 1-, 3-, and, 4-week cells ($P \leq 0.047$). Statistics: two-way repeated measures analysis of variance, Tukey post hoc test (**B**, **C**). Data presented as mean ± standard error of the mean.

localization along neurites. Here, we found PSD-95 is more abundant in somas relative to neurites during the first 2 weeks, but between 3 and 4 weeks, PSD-95 increasingly accumulates along hRGC neurites (Fig. 2). Similarly, other synaptic proteins, including synapsin-1, vGlut2, SNAP25, and neurexin-1, increase along hRGC neurites with time in culture.[26] Thus, hRGCs seem to possess the basic hardware to drive synaptic plasticity, including PSD-95 and glutamatergic receptors, suggesting that these mechanisms may be intrinsically pliable or exogenously controlled to achieve synaptic integration into recipient retinas.

Human RGC Physiologic Development

Our key physiologic finding is that hRGC voltage-gated responses increase and spike thresholds decrease over culture duration (Figs. 5, 6). This result is important for defining the physiologic maturity of hRGCs for testing the efficacy of potential therapeutics for optic neuropathies that modulate excitability. However, throughout the developmental time course studied here, hRGCs often produced few full spikes in response to depolarizing currents relative to mature native RGCs from whole retinas.[31,51] Instead, prolonged current stimulation often evoked a few full spikes followed by aborted action potentials and maintained depolarization (Fig. 5A). This response is typical of depolarization block[21,52–54] that has previously been reported in hRGCs.[21] Depolarization block is generally thought to protect neurons from excessive excitability[53] and may be dependent on presynaptic inputs driving postsynaptic membrane potential and intrinsic factors, including intracellular adenosine triphosphate (ATP) levels, NaV channel activity, and AIS length and NaV channel localization.[21,52,54,55]

Considering our experimental conditions and the intrinsic properties of hRGCs, we attempt to explain the cause for the low threshold for depolarization block. In our physiologic experiments hRGCs received a continuous supply of ATP through the intracellular pipette solution (4 mM Mg-ATP). Therefore, ATP depletion is not likely the cause for depolarization block. Second, pre-synaptic inputs are not likely to lower the threshold for depolarization block. Although neurites from multiple hRGCs seem to intersect (Fig. 1B), hRGCs intrinsically generate few excitatory postsynaptic currents.[26,56] Third, the inactivation of NaV channels may cause depolarization block.[21,55] We tested this idea directly by injecting a series of conditioning potentials to inactivate NaV channels followed by a test potential to determine the remaining available channels (Fig. 7A). We found the fraction of available channels is similar for most conditioning potentials with the exception that 7-week cells have more inactivated channels at –50 mV (Fig. 7C). These data indicate that NaV inactivation is not the sole cause for depolarization block.

Instead, we propose that the depolarization block occurs because hRGCs possess few NaV channels, specifically NaV1.6 channels, to support repetitive spiking.[44] This idea is reinforced by low mRNA expression of SCN8A, which encodes NaV1.6 protein (Fig. 3B). Depolarization block occurs at relatively modest currents also in dopaminergic neurons of the substantia nigra, which have small somatic NaV

conductance.[57,58] Finally, although we find the AIS scaffolding protein, AnkG, clusters along putative axons late in culture, the AIS does not seem to be well-formed (Fig. 3D). Therefore, we predict that voltage-gated channels recruited to the AIS, such as NaV1.6, are also unorganized, impairing normal action potential firing.[59]

Acknowledgments

The authors thank Louis-Philippe Croteau for helpful discussions and Catherine Formichella for imaging.

Supported by a departmental unrestricted award by the Research to Prevent Blindness Inc., Research to Prevent Blindness Inc. Stein Innovation Award, the Stanley Cohen Innovation Fund, and National Institutes of Health grants EY017427 (DJC), EY024997 (DJC), EY008126 (DJC), and EY029903 (JLG, DJC, DJZ). Imaging supported through the Vanderbilt University Medical Center Cell Imaging Shared Resource core facility and NIH grants CA68485, DK20593, DK58404, and DK59637.

Disclosure: **M.L. Risner**, None; **S. Pasini**, None; **X. Chamling**, None; **N.R. McGrady**, None; **J.L. Goldberg**, None; **D.J. Zack**, None; **D.J. Calkins**, None

References

1. Burgoyne CF. A biomechanical paradigm for axonal insult within the optic nerve head in aging and glaucoma. *Exp Eye Res.* 2011;93(2):120–132.
2. Calkins DJ. Critical pathogenic events underlying progression of neurodegeneration in glaucoma. *Prog Retin Eye Res.* 2012;31(6):702–719.
3. Leske MC, Heijl A, Hussein M, Bengtsson B, Hyman L, Komaroff E. Factors for glaucoma progression and the effect of treatment: the early manifest glaucoma trial. *Arch Ophthalmol.* 2003;121(1):48–56.
4. Wareham LK, Risner ML, Calkins DJ. Protect, repair, and regenerate: towards restoring vision in glaucoma. *Curr Ophthalmol Rep.* 2020;8(4):301–310.
5. Chamling X, Sluch VM, Zack DJ. The potential of human stem cells for the study and treatment of glaucoma. *Invest Ophthalmol Vis Sci.* 2016;57(5):ORSFi1–ORSFi6.
6. Chang EE, Goldberg JL. Glaucoma 2.0: neuroprotection, neuroregeneration, neuroenhancement. *Ophthalmology.* 2012;119(5):979–986.
7. Ohlemacher SK, Langer KB, Fligor CM, Feder EM, Edler MC, Meyer JS. Advances in the differentiation of retinal ganglion cells from human pluripotent stem cells. *Adv Exp Med Biol.* 2019;1186:121–140.
8. Stern JH, Tian Y, Funderburgh J, et al. Regenerating eye tissues to preserve and restore vision. *Cell Stem Cell.* 2018;22(6):834–849.
9. Johnson TV, Bull ND, Hunt DP, Marina N, Tomarev SI, Martin KR. Neuroprotective effects of intravitreal mesenchymal stem cell transplantation in experimental glaucoma. *Invest Ophthalmol Vis Sci.* 2010;51(4):2051–2059.
10. da Silva-Junior AJ, Mesentier-Louro LA, Nascimento-Dos-Santos G, et al. Human mesenchymal stem cell therapy promotes retinal ganglion cell survival and target reconnection after optic nerve crush in adult rats. *Stem Cell Res Ther.* 2021;12(1):69.
11. Sluch VM, Davis CH, Ranganathan V, et al. Differentiation of human ESCs to retinal ganglion cells using a CRISPR engineered reporter cell line. *Sci Rep.* 2015;5:16595.
12. Sluch VM, Chamling X, Liu MM, et al. Enhanced stem cell differentiation and immunopurification of genome engineered human retinal ganglion cells. *Stem Cells Transl Med.* 2017;6(11):1972–1986.
13. Gan L, Xiang M, Zhou L, Wagner DS, Klein WH, Nathans J. POU domain factor Brn-3b is required for the development of a large set of retinal ganglion cells. *Proc Natl Acad Sci USA.* 1996;93(9):3920–3925.
14. Zhang X, Tenerelli K, Wu S, et al. Cell transplantation of retinal ganglion cells derived from hESCs. *Restor Neurol Neurosci.* 2020;38(2):131–140.
15. Daniszewski M, Senabouth A, Nguyen QH, et al. Single cell RNA sequencing of stem cell-derived retinal ganglion cells. *Sci Data.* 2018;5:180013.
16. Lamba DA, MO Karl, Ware CB, Reh TA. Efficient generation of retinal progenitor cells from human embryonic stem cells. *Proc Natl Acad Sci USA.* 2006;103(34):12769–12774.
17. Ohlemacher SK, Sridhar A, Xiao Y, et al. Stepwise differentiation of retinal ganglion cells from human pluripotent stem cells enables analysis of glaucomatous neurodegeneration. *Stem Cells.* 2016;34(6):1553–1562.
18. Langer KB, Ohlemacher SK, Phillips MJ, et al. Retinal ganglion cell diversity and subtype

specification from human pluripotent stem cells. *Stem Cell Reports.* 2018;10(4):1282–1293.
19. Sanes JR, Masland RH. The types of retinal ganglion cells: current status and implications for neuronal classification. *Annu Rev Neurosci.* 2015;38:221–246.
20. Tanaka T, Yokoi T, Tamalu F, Watanabe S, Nishina S, Azuma N. Generation of retinal ganglion cells with functional axons from human induced pluripotent stem cells. *Sci Rep.* 2015;5:8344.
21. Teotia P, Van Hook MJ, Fischer D, Ahmad I. Human retinal ganglion cell axon regeneration by recapitulating developmental mechanisms: effects of recruitment of the mTOR pathway. *Development.* 2019;146(13):dev178012.
22. Venugopalan P, Cameron EG, Zhang X, Nahmou M, Muller KJ, Goldberg JL. Physiologic maturation is both extrinsically and intrinsically regulated in progenitor-derived neurons. *Sci Rep.* 2020;10(1):2337.
23. Wang DD, Kriegstein AR. GABA regulates excitatory synapse formation in the neocortex via NMDA receptor activation. *J Neurosci.* 2008;28(21):5547–5558.
24. Gill KP, Hung SS, Sharov A, et al. Enriched retinal ganglion cells derived from human embryonic stem cells. *Sci Rep.* 2016;6:30552.
25. Teotia P, Van Hook MJ, Wichman CS, Allingham RR, Hauser MA, Ahmad I. Modeling glaucoma: retinal ganglion cells generated from induced pluripotent stem cells of patients with SIX6 risk allele show developmental abnormalities. *Stem Cells.* 2017;35(11):2239–2252.
26. VanderWall KB, Vij R, Ohlemacher SK, et al. Astrocytes regulate the development and maturation of retinal ganglion cells derived from human pluripotent stem cells. *Stem Cell Reports.* 2019;12(2):201–212.
27. Leterrier C. The axon initial segment: an updated viewpoint. *J Neurosci.* 2018;38(9):2135–2145.
28. Huang CY, Rasband MN. Axon initial segments: structure, function, and disease. *Ann N Y Acad Sci.* 2018;1420(1):46–61.
29. Kim D, Langmead B, Salzberg SL. HISAT: a fast spliced aligner with low memory requirements. *Nat Methods.* 2015;12(4):357–360.
30. Trapnell C, Williams BA, Pertea G, et al. Transcript assembly and quantification by RNA-Seq reveals unannotated transcripts and isoform switching during cell differentiation. *Nat Biotechnol.* 2010;28(5):511–515.
31. Risner ML, McGrady NR, Boal AM, Pasini S, Calkins DJ. TRPV1 aupports axogenic enhanced excitability in response to neurodegenerative stress. *Front Cell Neurosci.* 2020;14:603419.
32. Fischer RA, Risner ML, Roux AL, Wareham LK, Sappington RM. Impairment of membrane repolarization accompanies axon transport deficits in glaucoma. *Front Neurosci.* 2019;13:1139.
33. Risner ML, Pasini S, Cooper ML, Lambert WS, Calkins DJ. Axogenic mechanism enhances retinal ganglion cell excitability during early progression in glaucoma. *Proc Natl Acad Sci USA.* 2018;115(10):E2393–e2402.
34. Rodriguez AR, de Sevilla Müller LP, Brecha NC. The RNA binding protein RBPMS is a selective marker of ganglion cells in the mammalian retina. *J Comp Neurol.* 2014;522(6):1411–1443.
35. Wong WT, Wong RO. Changing specificity of neurotransmitter regulation of rapid dendritic remodeling during synaptogenesis. *Nat Neurosci.* 2001;4(4):351–352.
36. Leterrier C, Dargent B. No Pasaran! Role of the axon initial segment in the regulation of protein transport and the maintenance of axonal identity. *Semin Cell Dev Biol.* 2014;27:44–51.
37. Van Wart A, Boiko T, Trimmer JS, Matthews G. Novel clustering of sodium channel Na(v)1.1 with ankyrin-G and neurofascin at discrete sites in the inner plexiform layer of the retina. *Mol Cell Neurosci.* 2005;28(4):661–673.
38. Boiko T, Van Wart A, Caldwell JH, Levinson SR, Trimmer JS, Matthews G. Functional specialization of the axon initial segment by isoform-specific sodium channel targeting. *J Neurosci.* 2003;23(6):2306–2313.
39. Margolis DJ, Gartland AJ, Euler T, Detwiler PB. Dendritic calcium signaling in ON and OFF mouse retinal ganglion cells. *J Neurosci.* 2010;30(21):7127–7138.
40. Mitra P, Miller RF. Normal and rebound impulse firing in retinal ganglion cells. *Vis Neurosci.* 2007;24(1):79–90.
41. Jahnsen H, Llinás R. Electrophysiological properties of guinea-pig thalamic neurones: an in vitro study. *J Physiol.* 1984;349:205–226.
42. Liao Y-F, Tsai M-L, Chen C-C, Yen C-T. Involvement of the Cav3.2 T-type calcium channel in thalamic neuron discharge patterns. *Mol Pain.* 2011;7:43–43.
43. Azouz R, Gray CM. Dynamic spike threshold reveals a mechanism for synaptic coincidence detection in cortical neurons in vivo. *Proc Natl Acad Sci USA.* 2000;97(14):8110–8115.
44. Rush AM, Dib-Hajj SD, Waxman SG. Electrophysiological properties of two axonal sodium channels, Nav1.2 and Nav1.6, expressed in mouse

spinal sensory neurones. *J Physiol.* 2005;564(Pt 3):803–815.
45. VanderWall KB, Huang KC, Pan Y, et al. Retinal ganglion cells with a glaucoma OPTN(E50K) mutation exhibit neurodegenerative phenotypes when derived from three-dimensional retinal organoids. *Stem Cell Reports.* 2020;15(1):52–66.
46. Raghuram V, Werginz P, Fried SI. Scaling of the AIS and somatodendritic compartments in α S RGCs. *Front Cell Neurosci.* 2019;13:436.
47. Wong WT, Faulkner-Jones BE, Sanes JR, Wong RO. Rapid dendritic remodeling in the developing retina: dependence on neurotransmission and reciprocal regulation by Rac and Rho. *J Neurosci.* 2000;20(13):5024–5036.
48. Sans N, Petralia RS, Wang YX, Blahos J, 2nd, Hell JW, Wenthold RJ. A developmental change in NMDA receptor-associated proteins at hippocampal synapses. *J Neurosci.* 2000;20(3):1260–1271.
49. Buonarati OR, Hammes EA, Watson JF, Greger IH, Hell JW. Mechanisms of postsynaptic localization of AMPA-type glutamate receptors and their regulation during long-term potentiation. *Sci Signal.* 2019;12(562):eaar6889, doi:10.1126/scisignal.aar6889.
50. Han K, Kim E. Synaptic adhesion molecules and PSD-95. *Prog Neurobiol.* 2008;84(3):263–283.
51. Reinhard K, Münch TA. Visual properties of human retinal ganglion cells. *PLoS One.* 2021;16(2):e0246952.
52. Werginz P, Raghuram V, Fried SI. Tailoring of the axon initial segment shapes the conversion of synaptic inputs into spiking output in OFF-α T retinal ganglion cells. *Sci Adv.* 2020;6(37):eabb6642, doi:10.1126/sciadv.abb6642.
53. Bianchi D, Marasco A, Limongiello A, et al. On the mechanisms underlying the depolarization block in the spiking dynamics of CA1 pyramidal neurons. *J Comput Neurosci.* 2012;33(2):207–225.
54. Knauer B, Yoshida M. Switching between persistent firing and depolarization block in individual rat CA1 pyramidal neurons. *Hippocampus.* 2019;29(9):817–835.
55. Kuznetsova AY, Huertas MA, Kuznetsov AS, Paladini CA, Canavier CC. Regulation of firing frequency in a computational model of a midbrain dopaminergic neuron. *J Comput Neurosci.* 2010;28(3):389–403.
56. Riazifar H, Jia Y, Chen J, Lynch G, Huang T. Chemically induced specification of retinal ganglion cells from human embryonic and induced pluripotent stem cells. *Stem Cells Transl Med.* 2014;3(4):424–432.
57. Seutin V, Engel D. Differences in Na+ conductance density and Na+ channel functional properties between dopamine and GABA neurons of the rat substantia nigra. *J Neurophysiol.* 2010;103(6):3099–3114.
58. Tucker KR, Huertas MA, Horn JP, Canavier CC, Levitan ES. Pacemaker rate and depolarization block in nigral dopamine neurons: a somatic sodium channel balancing act. *J Neurosci.* 2012;32(42):14519–14531.
59. Zhou D, Lambert S, Malen PL, Carpenter S, Boland LM, Bennett V. AnkyrinG is required for clustering of voltage-gated Na channels at axon initial segments and for normal action potential firing. *J Cell Biol.* 1998;143(5):1295–1304.